Monthly Notices of the ROYAL ASTRONOMICAL SOCIETY LETTERS

Mon. Not. R. Astron. Soc. **406,** L45–L49 (2010) doi:10.1111/j.1745-3933.2010.00878.x

Microwave observations of spinning dust emission in NGC 6946★

AMI Consortium: Anna M. M. Scaife,[1]† Bojan Nikolic,[2,3] David A. Green,[3] Rainer Beck,[4] Matthew L. Davies,[3] Thomas M. O. Franzen,[3] Keith J. B. Grainge,[2,3] Michael P. Hobson,[3] Natasha Hurley-Walker,[3] Anthony N. Lasenby,[2,3] Malak Olamaie,[3] Guy G. Pooley,[3] Carmen Rodríguez-Gonzálvez,[3] Richard D. E. Saunders,[2,3] Paul F. Scott,[3] Timothy W. Shimwell,[3] David J. Titterington,[3] Elizabeth M. Waldram[3] and Jonathan T. L. Zwart[5]

[1]*Dublin Institute for Advanced Studies, 31 Fitzwilliam Place, Dublin 2, Ireland*
[2]*Kavli Institute for Cosmology Cambridge, Madingley Road, Cambridge CB3 0HA*
[3]*Astrophysics Group, Cavendish Laboratory, J J Thomson Avenue, Cambridge CB3 0HE*
[4]*MPIfR, Auf dem Hügel 69, 53121 Bonn, Germany*
[5]*Columbia Astrophysics Laboratory, Columbia University, 550 West 120th Street, NY 10027, USA*

Accepted 2010 May 15. Received 2010 May 14; in original form 2010 April 27

ABSTRACT

We report new cm-wave measurements at five frequencies between 15 and 18 GHz of the continuum emission from the reportedly anomalous 'region 4' of the nearby galaxy NGC 6946. We find that the emission in this frequency range is significantly in excess of that measured at 8.5 GHz, but has a spectrum from 15 to 18 GHz consistent with optically thin free–free emission from an ultracompact H II region. In combination with previously published data, we fit four emission models containing different continuum components using the Bayesian spectrum analysis package RADIOSPEC. These fits show that, in combination with data at other frequencies, a model with a spinning dust component is slightly preferred to those that possess better-established emission mechanisms.

Key words: radiation mechanisms: general – galaxies: individual: NGC 6946.

1 INTRODUCTION

The complete characterization of microwave emission from spinning dust grains is a key question in both astrophysics and cosmology as it probes a region of the electromagnetic spectrum where a number of different astrophysical disciplines overlap: it is important for cosmic microwave background observations in order to correctly characterize the contaminating foreground emission (Gold et al. 2010); for star and planetary formation, it is important because it potentially probes a regime of grain sizes that is not otherwise easily observable (Rafikov 2006).

Although a number of objects have now been found to exhibit anomalous microwave emission, attributed to spinning dust, it is still unclear what differentiates those objects from the many other seemingly similar targets that do not show the excess. In order to investigate this question, a number of Galactic observations have been made towards known star formation regions (e.g. Watson et al. 2005; Casassus et al. 2008; Scaife et al. 2010; Tibbs et al. 2010). In addition, Murphy et al. (2010, hereinafter M10) made the first extragalactic search for anomalous microwave emission within the star formation regions of the nearby galaxy NGC 6946 using the Caltech Continuum Back-end on the Green Bank Telescope. M10 found a significantly anomalous spectrum in only one of 10 star-forming regions: extranuclear region 4 (hereinafter NGC 6946-E4). The excess of emission was seen between 27 and 40 GHz relative to the continuum emission at 8.5 GHz measured using combined Effelsberg 100-m Telescope and Very Large Array (VLA) observations (Beck 2007).

In this Letter, we present follow-up observations of NGC 6946-E4 at frequencies from 15 to 18 GHz using the Arcminute Microkelvin Imager (AMI) Large Array (LA). In Section 2, we present the details of these observations; in Section 3, we present the results of the AMI-LA observations and a comparison with other radio data; and in Section 4, we discuss the implications of these results and form our conclusions. In what follows we use the convention $S \propto \nu^{\alpha}$, where S is the flux density, ν is the frequency and α is the spectral index. All errors are quoted to 1σ.

2 OBSERVATIONS

The AMI LA consists of eight 13-m antennas and is sited at Lord's Bridge, Cambridge. For technical details, see AMI Consortium: Zwart et al. (2008). The telescope observes in the band 13.9–18.2 GHz in eight 0.75-GHz bandwidth channels. In what follows,

★We request that any reference to this paper cites 'AMI Consortium: Scaife et al. 2010'.

†E-mail: ascaife@cp.dias.ie

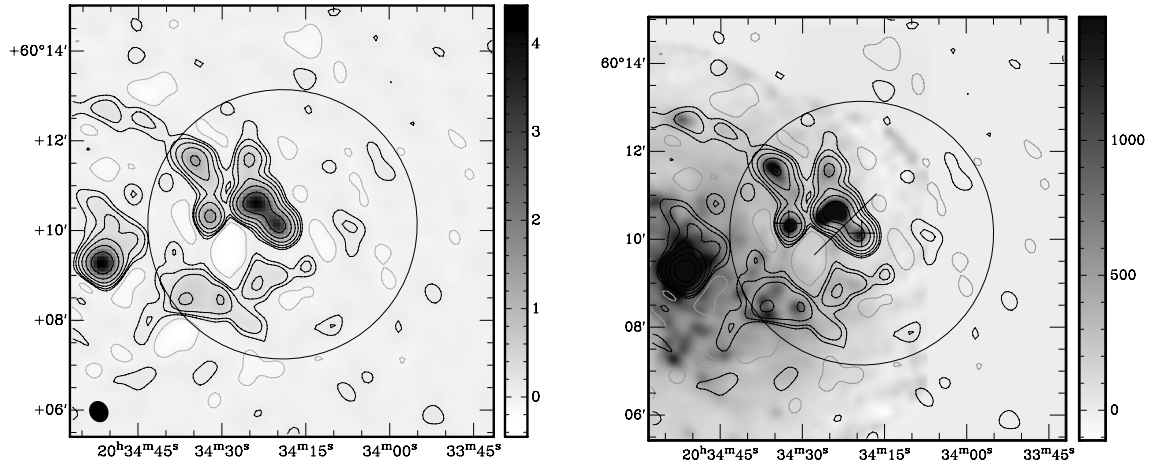

(a) (b)

Figure 1. NGC 6946-E4. (a) Grey-scale and contours at -3σ, 3σ, 6σ, 12σ, etc., are from the AMI LA, where $\sigma_{\rm rms} = 25$ μJy beam^{-1}; grey-scale units are mJy beam^{-1}. Data are not corrected for the primary beam response. The AMI-LA synthesized beam, 29.2×25.2 arcsec^2, is shown as a filled ellipse in the bottom-left corner. (b) Contours are from the AMI LA and grey-scale at 8.5 GHz is from Effelsberg-VLA measurements; grey-scale units are μJy beam^{-1} (Beck 2007). The positions of NGC 6946-E4 (at the phase centre) and NGC 6946-E8 (to the east) are marked with crosses, and a line is drawn to indicate a non-fitted polygon edge (see the text for details). The AMI-LA primary beam is shown as a black circle in both images.

the three lowest frequency channels (1, 2 and 3; 13.9–14.6 GHz) are not used due to interference from geostationary satellites.

NGC 6946-E4 (J 20$^{\rm h}$34$^{\rm m}$19$^{\rm s}$.17 + 60°10′08″.7) was observed by the AMI LA in a single 12-h synthesis. Data reduction was performed using the local software tool REDUCE. This applies both automatic and manual flags for interference, shadowing and hardware errors, phase and amplitude calibrations before output to disk in *uv* FITS format suitable for imaging in AIPS. Flux calibration was performed using short observations of 3C 48 at the beginning of the run and 3C 286 at the end. We assumed $I+Q$ flux densities for these sources in the AMI-LA channels consistent with the frequency-dependent model of Baars et al. (1977), $\simeq$1.64 and 3.48 Jy, respectively, at 15 GHz. As Baars et al. measure I and AMI LA measures $I+Q$, these flux densities include corrections for the polarization of the calibrator sources derived by interpolating from VLA 5-, 8- and 22-GHz observations. A correction is also made for the changing intervening airmass over the observation using the AMI 'raingauge' noise-injection system. The weather was good during the observation and no correction greater than 6 per cent was applied. From cross-calibration of 3C 48 and 3C 286, we find that the flux calibration is accurate to better than 5 per cent. The phase was calibrated using interleaved observations of J2031+5455, selected from the Jodrell Bank VLA Survey (JVAS; Patnaik et al. 1992). After calibration, the phase is generally stable to 5° for channels 4–7 and 10° for channel 8. Reduced data were imaged using the AIPS data package. CLEAN deconvolution was performed interactively using the task IMAGR with a loop gain of 5 per cent and clean boxes around field sources for approximately the first one-third of the iterations. CLEAN deconvolution maps were made both from the combined channel set and for individual channels. The full width at half-maximum (FWHM) of the primary beam of the AMI LA is ≈6 arcmin at 16 GHz.

3 RESULTS

3.1 AMI-LA data

The combined channel map from the AMI-LA observation of NGC 6946-E4 is shown in Fig. 1. E4 is located at the phase centre with extranuclear region 8 (J20$^{\rm h}$34$^{\rm m}$32$^{\rm s}$.52 + 60°10′22″.0; NGC 6946-E8) to the east and the galactic nucleus of NGC 6946 (J20$^{\rm h}$34$^{\rm m}$52$^{\rm s}$.34 +60°09′14″.2) further to the east, outside the primary beam FWHM. Since NGC 6946-E8 also lies within the FWHM of the primary beam, we used the recovered flux densities for this source as a check on the absolute calibration for this field. Flux densities were extracted using the FITFLUX software (Green 2007; AMI Consortium: Scaife et al. 2009) using the primary-beam-corrected maps. This method calculates flux densities by removing a tilted plane fitted to the local background and integrating the remaining flux. We do this by drawing a polygon around the source and fitting a tilted plane to the pixels around the edge of the polygon. Where an edge of the polygon crosses a region confused by another source, the background is subjective and we omit this edge from the fitting. An example of where this might be appropriate is shown in Fig. 1(b). Since the extracted flux density is dependent to some degree on the background emission, we repeat this process using five irregular polygons, each varying slightly in shape. The final flux density is the average of that extracted from these five polygons.

Errors on the flux densities were calculated as $\sigma_\nu = \sqrt{(0.05S_\nu)^2 + \sigma^2_{{\rm rms},\nu} + \sigma^2_{\rm fit}}$, where $\sigma_{{\rm rms},\nu}$ is the rms noise outside the primary beam on each channel map and $\sigma_{\rm fit}$ is the standard deviation of the fluxes measured in the five polygonal apertures. The errors are dominated by $\sigma_{\rm fit}$, which is large due to the complicated background emission in this crowded field. The flux densities measured for NGC 6946-E4 and 6946-E8 are listed in Table 1.

3.2 NCC6946-E4: comparison with other radio data

We compared the AMI-LA data with those at 8.5 GHz from the Effelsberg 100 -m and VLA telescopes (Beck 2007). These data in their original form (see Fig. 1b), constitute a total power measurement of the region at a resolution of 15 arcsec. We Fourier transformed these combined data and sampled them at *uv* positions identical to those of the AMI-LA 15.0-GHz data (channel 4) in order to compare consistent angular scales. The resulting *uv* data set was then mapped and cleaned in the same way as the AMI-LA data. Since channel 4 of the AMI LA recovers a large amount of

Table 1. Flux densities.

Source	8.5 GHz	AMI-LA channel number 4 (15.0 GHz)	5 (15.4 GHz)	6 (16.4 GHz)	7 (17.2 GHz)	8 (17.9 GHz)
	(mJy)	(mJy)	(mJy)	(mJy)	(mJy)	(mJy)
(1)	(2)	(3)	(4)	(5)	(6)	(7)
NGC 6946-E4	1.94 ± 0.29	3.17 ± 0.36	3.16 ± 0.33	3.00 ± 0.28	3.15 ± 0.43 (3.31 ± 0.43)	2.78 ± 0.34 (3.09 ± 0.35)
NGC 6946-E8	2.11 ± 0.21	1.90 ± 0.27	1.51 ± 0.27	1.40 ± 0.23	1.51 ± 0.34	1.42 ± 0.19

Note. Column (1) contains the source name, (2) the *uv*-sampled 8.5-GHz flux density for that source and (3)–(8) contain the AMI-LA flux densities for each source from AMI-LA channels 4–8, with flux-loss-corrected values in parentheses.

the extended structure around NGC 6946-E4, the flux density for this source from the sampled 8.5-GHz map is very similar to the unsampled value (see Table 1).

Since the *uv* coverage of the AMI LA varies across the frequency channels, we quantified the amount of flux lost in each channel relative to channel 4 by sampling the total power 8.5-GHz map to match the *uv* coverage in each of the AMI-LA frequency channels. This showed that flux loss was negligible in channels 4–6 and notable in channels 7 (5 per cent) and 8 (10 per cent) only. We corrected for this loss in the measured AMI-LA flux densities with corrected values shown in parentheses in Table 1. In the same manner, we checked for corrections to the flux densities of NGC 6946-E8. In this case, the corrections were negligible (<2 per cent) and no corrections were made. We found the AMI-LA data for NGC 6946-E8 to be consistent with the spectrum for this object presented in M10. The flux density of NGC 6946-E4 across the AMI-LA band is in excess of the 8.5-GHz flux density by $\sim 10\sigma$.

The collected observations of both regions E4 and E8 were analysed using an updated version of the RADIOSPEC package[1] (Nikolic 2009). This software tool calculates the posterior distribution and the Bayesian evidence for a given model. The implementation of these calculations is based on the nested sampling algorithm by Skilling (2004). For the analysis of the data in this Letter, we used several different models, each of which consists of a number of components, each with physically parametrized properties. Two components that are present in all models are a synchrotron component, parametrized in terms of the supernova rate within the beam, and an unabsorbed free–free component, parametrized in terms of the star formation rate within the beam ($SFR_{\rm unabs}$). The conversions from these physical parameters to radio luminosities are made according to the formulae given by Condon (1992).

In order to explain the excess of emission at cm wavelengths, it is necessary to introduce another component that contributes to the emission. As outlined above, we have considered two options: emission due to spinning dust and absorbed free–free emission from an ultracompact H II (UCHII) region. For the spinning dust emission component, we used the warm ionized medium model described by Draine & Lazarian (1998).[2]

The only degree of freedom in this model is the overall amplitude, which we parametrized in terms of the total mass of gas, $M_{\rm gas}$, carrying the spinning dust. There have been a number of recent updates to this model (Ali-Haïmoud, Hirata & Dickinson 2009; Ysard & Verstraete 2010); however, a complete comparison is beyond the scope of this Letter.

Our model for the absorbed free–free emission from H II is again parametrized in terms of the star formation rate in the region ($SFR_{\rm abs}$) and also the filling factor, f, i.e. the fraction of the area covered by the telescope beam that the H II region subtends, as a free parameter. This area is used to compute the free–free opacity as a function of frequency and to correct the unabsorbed free–free model for the effects of absorption.

Considered on their own, the AMI-LA data (after correction for flux loss) have a spectral index of $\alpha_{\rm AMI} = -0.11 \pm 0.77$. Although this value is consistent with optically thin free–free emission, the error is large and we cannot rule out other mechanisms. Since the spectral index between the Effelsberg-VLA measurement at 8.5 GHz and the AMI band is rising ($\alpha_{8.5}^{16} = 0.67 \pm 0.08$; see Fig. 2), we need to consider the possibility that region E4 contains one or more UCHII regions with their opacity reaching unity at $\sim$12 GHz. Such an opacity would require an emission measure of $\simeq 5 \times 10^8$ pc cm^{-6}, assuming $T_{\rm e} = 10^4$ K, and would be appropriate for a UCHII region.

We therefore examine two alternative hypotheses for the emission from region E4. The first is that the emission is due to the usual diffuse synchrotron and free–free mechanisms associated with star formation, with an additional high-opacity free–free component (hypothesis 1; H1). The second hypothesis includes a spinning dust component rather than high-opacity free–free (H2). A summary of how well these two hypotheses fit the observed data is shown in the form of fan diagrams in Fig. 2. As can be seen from this figure, neither of the hypotheses can be ruled out with the current data, although the spinning dust model appears to somewhat better match the data. This is also confirmed by a simple comparison of the models: assuming flat priors and no a priori difference between the models, the logarithmic Bayes factor is 3.7 ± 0.3 in favour of the spinning dust model. From the Jeffreys' scale of evidence (Jeffreys 1961; Kass & Raftery 1995; see e.g. Efron & Gous 2001 for further discussion of this scale), this would indicate a weak positive preference for the spinning dust model above the free–free model. The maximum likelihood parameters for these models are listed in Table 2.

For comparison, we have also carried out a similar analysis on region E8 (Fig. 3). In this case, the two hypotheses are a simple diffuse synchrotron plus free–free model (H1) and the same model with an additional spinning dust component (H2). In this case, the logarithm of the Bayesian evidence ratio is 0.5 ± 0.3 in favour of the simpler model without the spinning dust. A ratio of this size indicates no perceptible difference between the two models.

In region E4 where a spinning dust model is the preferred hypothesis we can marginalize the posterior distribution of the model parameters to obtain an estimate of the gas mass containing the

[1]The complete code and data used for this spectrum analysis are available for public download under GPL license: http://www.mrao.cam.ac.uk/~bn204/galevol/speca/sdgals.html.

[2] ftp://ftp.astro.princeton.edu/draine/dust/spin/emit4.jnu.wim_a

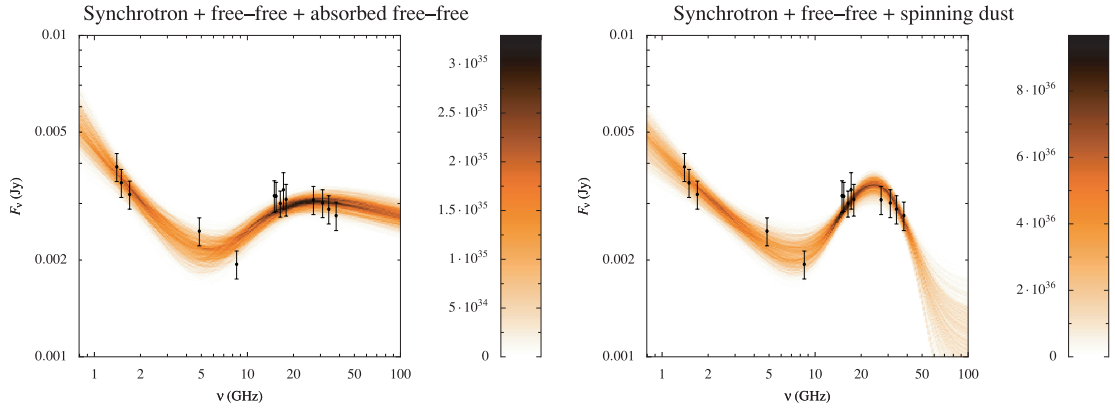

Figure 2. The observed radio spectrum of region E4 of NGC 6946 (points and error bars) with the fan diagram of two model fits to these data: on the left is the model with a highly absorbed free–free emission region (H1) and on the right is the model with spinning dust emission (H2). Low-frequency data are taken from M10, scaled to the *uv*-sampled flux density at 8.5 GHz, with the exception of points between 15 and 18 GHz which are from the AMI LA (this work). The assumed error is 10 per cent unless stated otherwise in Table 1. The colour scale indicates the evidence contribution as a function of frequency and flux density (for details, see Nikolic 2009).

Table 2. Derived model parameters and errors.

Model	SNe rate $\log_{10}(\mathrm{yr}^{-1})$ (2)	α_{sync} (3)	SFR_{abs} $\log_{10}(\mathrm{yr}^{-1})$ (4)	SFR_{unabs} $\log_{10}(\mathrm{yr}^{-1})$ (5)	M_{gas} $\log_{10}(\mathrm{M}_\odot)$ (6)	f $\log_{10}$(sterad) (7)	(χ^2, d.o.f.) (8)
Prior	$(-5, -1)$	$(-1.0, -0.5)$	$(-3, -1)$	$(-3, 0)$	(5, 9)	$(-6, -3)$	
NGC 6946-E4 (H1)	-3.84 ± 0.11	-0.74 ± 0.14	-0.93 ± 0.07	-1.80 ± 0.48	–	-4.97 ± 0.18	(9.1, 8)
NGC 6946-E4 (H2)	-3.98 ± 0.16	-0.71 ± 0.15	–	-1.40 ± 0.36	8.12 ± 0.09	–	(5.5, 9)
NGC 6946-E8 (H1)	-3.65 ± 0.04	-0.66 ± 0.13	–	-1.70 ± 0.41	–	–	(4.6,1 0)
NGC 6946-E8 (H2)	-3.64 ± 0.04	-0.65 ± 0.12	–	-1.75 ± 0.41	6.19 ± 0.66	–	(4.6, 9)

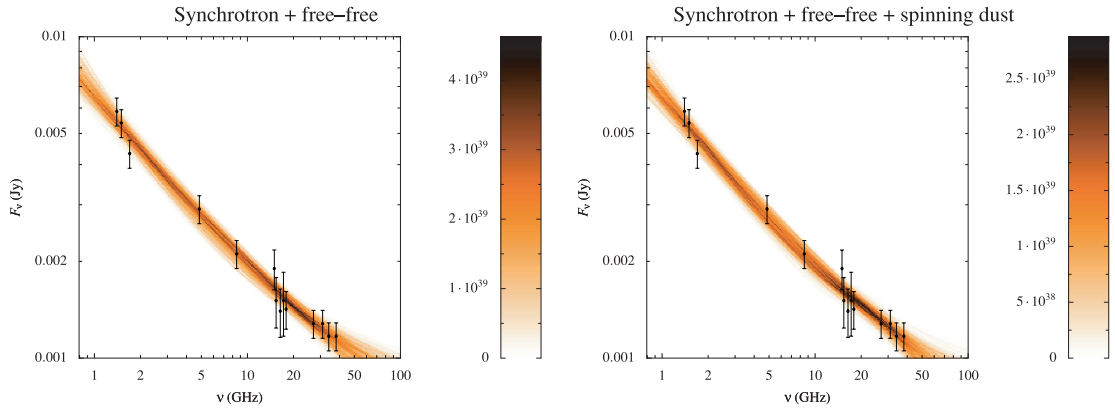

Figure 3. The observed radio spectrum and fan diagrams for region E8 of NGC 6946, with data and errors as in Fig. 2. The model on the left-hand side only consists of a synchrotron and unabsorbed free–free components (H1), while the model on the right-hand side also has a spinning dust component (H2). Low-frequency data are taken from M10, scaled to the *uv*-sampled flux density at 8.5 GHz, with the exception of points between 15 and 18 GHz which are from the AMI LA (this work). The assumed error is 10 per cent unless stated otherwise in Table 1. The colour scale is as above.

spinning dust, shown as a histogram in the left-hand panel of Fig. 4 and in a numerical form in Table 2, i.e. $10^{8.1\pm0.1}\,\mathrm{M}_\odot$. In region E8 spinning dust is not the preferred hypothesis but proceeding with this hypothesis anyway, we find an upper limit for the mass of the gas bearing the spinning dust, which is around $10^{7.5}\,\mathrm{M}_\odot$. We draw a conclusion that if the conditions in E4 and E8 are similar, then the mass of any gas bearing spinning dust in E8 must be at least a factor of 5 smaller than in E4.

Region E4 is located on the dense rim of a 'remarkable' H I hole (Boomsma et al. 2008) within NGC 6946. Such an association may be relevant to the differentiation of this star formation region from the eight others found to exhibit no anomalous emission by M10. The hole is remarkable for a number of reasons, notably the almost unbroken symmetry of its dense H I rim, unusual in so large a hole, and the small-scale high-velocity gas complexes observed in connection with it.

4 CONCLUSIONS

The spinning dust model is preferred by the evidence calculation for NGC 6946-E4, but not at a very high level. Definitive confirmation of the nature of the emission requires measurements at frequencies

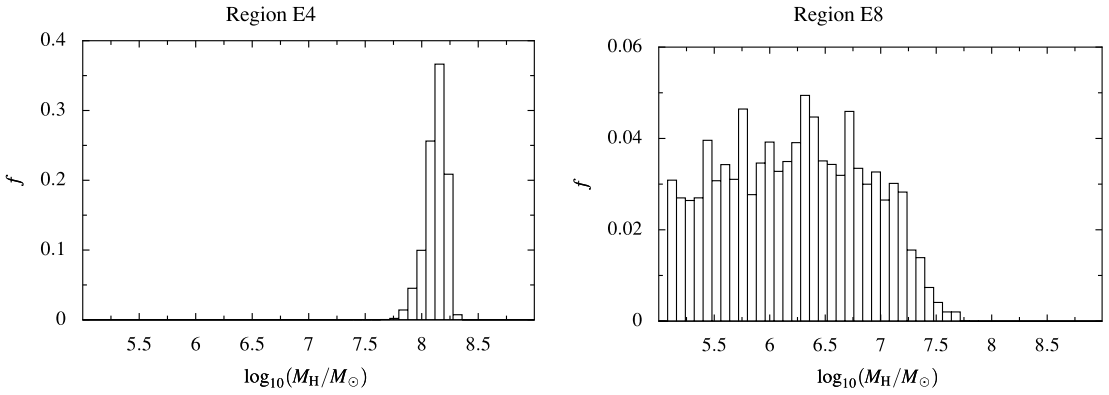

Figure 4. Marginalized distribution of inferred gas mass that bears the spinning dust: the left-hand panel shows extranuclear region 4 and the right-hand panel extranuclear region 8.

above 50 GHz, where the spinning dust and UCHII region models have significantly different behaviour. For example, Fig. 2 shows that at 100 GHz the difference between these two models should be at least a factor of 2 in brightness.

In the sub-mm there are data available from Submillimetre Common-User Bolometer Array (SCUBA) at 850 μm for this region by Di Francesco et al. (2008), which might be used to constrain the mass of NGC 6946-E4 and place constraints on the frequency at which the optical depth reaches unity. If a UCHII region is present, with $\tau = 1$ at $\nu > 8.5$ GHz it should have a correspondingly high dust mass. From analysis of the SCUBA data, we obtained a flux estimate for region E4 of $S_{850} = 11 \pm 14$ mJy beam^{-1}. However, the errors on this estimate are too high to allow any useful constraint on the properties of the thermal dust emission or to calculate a reliable dust mass estimate.

From the existing data the possibility of a spinning dust component in this region cannot be ruled out, but the evidence is not yet definitive. Further observations of this object at frequencies covering the higher frequency minimum between spinning dust emission and thermal dust emission (≈90 GHz) would be most useful, as would improved sub-mm data or alternatively sensitive RRL measurements in order to place strong constraints on the free–free emission.

ACKNOWLEDGMENTS

We thank the staff of the Lord's Bridge Observatory for their invaluable assistance in the commissioning and operation of the Arcminute Microkelvin Imager. The AMI LA is supported by Cambridge University and the STFC. AMMS thanks Thijs van der Hulst for drawing attention to the H I complexes in NGC 6946. CRG, TWS, TMOF, MO and MLD acknowledge the support of PPARC/STFC studentships.

REFERENCES

Ali-Haïmoud Y., Hirata C. M., Dickinson C., 2009, MNRAS, 395, 1055
AMI Consortium: Scaife A. M. M. et al., 2009, MNRAS, 400, 1394
AMI Consortium: Scaife A. M. M. et al., 2010, MNRAS, L16
AMI Consortium: Zwart J. T. L. et al., 2008, MNRAS, 391, 1545
Baars J. W. M., Genzel R., Pauliny-Toth I. I. K., Witzel A., 1977, A&A, 61, 99
Beck R., 2007, A&A, 470, 539
Boomsma R. et al., 2008, A&A, 490, 555
Casassus S. et al., 2008, MNRAS, 391, 1075
Condon J. J., 1992, ARA&A, 30, 575
Di Francesco J. et al., 2008, ApJS, 175, 277
Draine B. T., Lazarian A., 1998, ApJ, 508, 157
Efron B., Gous A., 2001, in Lahiri P., ed., Model Selection. Institute of Mathematical Statistics, Beachwood, OH, p. 208
Gold B. et al., 2010, preprint (arXiv:1001.4555)
Green D. A., 2007, Bull. Astron. Soc. India, 35, 77
Jeffreys H., 1961, Theory of Probability, 3rd edn. Oxford Univ. Press, Oxford
Kass R. E., Raftery A. E., 1995, J. American Statistical Association, 90, 773
Murphy E. J. et al., 2010, ApJ, 709, L108 (M10)
Nikolic B., 2009, preprint (arXiv:0912.2317)
Patnaik A. R., Browne I. W. A., Wilkinson P. N., Wrobel J. M., 1992, MNRAS, 254, 655
Rafikov R. R., 2006, ApJ, 646, 288
Skilling J., 2004, in Fischer R., Preuss R., von Toussaint U., eds, AIP Conf. Proc. Vol. 735, Nested Sampling, Bayesian Inference and Maximum Entropy Methods in Science and Engineering. Am. Inst. Phys., New York, p. 395
Tibbs C. T. et al., 2010, MNRAS, 402, 1969
Watson R. A. et al., 2005, ApJ, 624, L89
Ysard N., Verstraete L., 2010, A&A, 509, 12

This paper has been typeset from a TEX/LATEX file prepared by the author.